# REPORT DOCUMENTATION PAGE

Form Approved
OMB No. 074-0188



| 1. AGENCY USE ONLY (Leave blank) | 2. REPORT DATE | 3. REPORT TYPE AND DATES COVERED |
|---|---|---|
| | Oct. 18, 2000 | Final Report, March 1998-February 2000 |

**4. TITLE AND SUBTITLE**
Drag Reduction for Turbulent Boundary Layer Flows Using an Oscillating Wall

**5. FUNDING NUMBERS**
F49620-98-1-0333

**6. AUTHOR(S)**
Bogard, D. G., Ball, K. S., and Wassen, E.

AFRL-SR-BL-TR-00-
0629

**7. PERFORMING ORGANIZATION NAME(S) AND ADDRESS(ES)**
The University of Texas at Austin Austin, TX 78712

**8. PERFORMING ORGANIZATION REPORT NUMBER**
TTCRL 00-2

**9. SPONSORING / MONITORING AGENCY NAME(S) AND ADDRESS(ES)**
AFOSR 801 N. Randolph St.
Arlington, VA 22203

**10. SPONSORING / MONITORING AGENCY REPORT NUMBER**

**11. SUPPLEMENTARY NOTES**
Contract monitor: Dr. Steven Walker

**12a. DISTRIBUTION / AVAILABILITY STATEMENT**

**DISTRIBUTION STATEMENT A**
**Approved for Public Release**
**Distribution Unlimited**

**12b. DISTRIBUTION CODE**

**13. ABSTRACT** *(Maximum 200 Words)*

This research program used experimental measurements and computational simulations to study the drag reduction, and the resulting effects on turbulence structure, for a turbulent wall flow subjected to lateral wall oscillations. Major objectives for this study were to establish wall oscillation conditions resulting in maximum drag reduction, and how the turbulence structure was altered so that this drag reduction was attained. Furthermore we were interested in the drag reduction performance over a range of Reynolds numbers, and the onset of the drag reduction at the start of the oscillating wall section, and the decay of drag reduction downstream of the oscillating wall. Our experiments showed the maximum drag reduction for an oscillating wall is 30%. Furthermore, the drag reduction reaches an asymptotic level with increasing wall oscillation velocity, with the maximum level occurring by approximately $\bar{W}_{xp} = 15$. Drag reduction performance was tested for Reynolds numbers of $Re_\theta$ = 500, 950, 1400 and 2400, and the performance was found to be independent of Reynolds number for this range. Experimental and computational studies of the turbulence structure showed the oscillating wall has dramatic effect in practically eliminating the streak structures. Furthermore, the burst and sweep structures were suppressed.

| 14. SUBJECT TERMS | 15. NUMBER OF PAGES |
|---|---|
| Wall turbulence, drag reduction, streaks, bursts, sweeps | 17 |
| | 16. PRICE CODE |

| 17. SECURITY CLASSIFICATION OF REPORT | 18. SECURITY CLASSIFICATION OF THIS PAGE | 19. SECURITY CLASSIFICATION OF ABSTRACT | 20. LIMITATION OF ABSTRACT |
|---|---|---|---|
| Unclassified | Unclassified | Unclassified | |

# Drag Reduction for Turbulent Boundary Layer Flows Using an Oscillating Wall

AFOSR Project
March 1998-February 2000

Final Report

David G. Bogard, Kenneth S. Ball, and Erik Wassen

Mechanical Engineering Department
The University of Texas at Austin

October 2000

Report No. TTCRL 00-2

# Introduction

Recent numerical and experimental studies indicate that a continuous lateral oscillation of the wall in turbulent boundary layer flows can reduce the drag by as much as 50%. This technique is easy to implement and the energy cost is relatively low. Previous experiments conducted in our laboratory using this technique have achieved up to 30% drag reduction. In the present study we investigate the optimum operating conditions for the lateral wall oscillations, the effects of Reynolds number, the development length at the onset of the oscillating surface, and the decay length following the oscillating surface.

Significant drag reduction induced by laterally oscillating walls has been predicted computationally by Jung, Mangiavacchi and Akhavan (1992) and by Baron and Quadrio (1996). Both these numerical simulations were at relatively low Reynolds number, $Re_\tau = 200$. Jung et al. simulated an oscillation of the main flow using oscillation frequencies ranging from $f^+ = 0.04$ to $f^+ = 0.002$ ($f^+ = fv/u_\tau^2$), with a constant lateral velocity peak amplitude. A wall oscillation was simulated for a frequency of $f^+ = 0.01$. A net reduction in the wall shear stress was obtained for $0.005 \le f^+ \le 0.04$. Maximum drag reduction as much as 40% was achieved at $f^+ = 0.01$, for both the oscillatory cross-flow case and the oscillatory channel wall case. Much lower drag reduction was predicted when the peak lateral velocity was decreased by a factor of two.

A similar numerical study was performed by Baron and Quadrio (1996). They examined the spanwise oscillating wall case only at a frequency of $f^+ = 0.01$, which was the frequency for maximum drag reduction according to the work by Jung *et al.* (1992). A variation of peak-to-peak oscillation amplitude was carried out in the study, ranging from $\Delta z^+ = 120$ to $\Delta z^+ = 480$. The same Reynolds number as used by Jung *et al.*, i.e. $Re_\tau = 200$ was used. A maximum drag reduction of 40% was found at the maximum amplitude of $\Delta z^+ = 480$, consistent with the results of Jung *et al.*

An experimental investigation was conducted by Laadhari, Skandaji and Morel (1994) to examine the drag reduction effect of the turbulent boundary layer on a flat plate subjected to a local spanwise oscillating wall. The experiment was performed in a wind tunnel with the boundary layer momentum thickness Reynolds number $Re_\theta = 950$. Lateral oscillations were at frequencies ranging $0.0033 \le f^+ \le 0.0166$. The peak-to-peak amplitude was $\Delta z^+ \approx 320$, which was slightly less than that examined by Jung *et al.* (1992). Although no drag reduction was quoted in this paper, the reduction in peak Reynolds shear stress was measured to be 20%.

Prior to the start of the AFOSR sponsored research in our laboratory, experiments were conducted to determine the effects of steady, lateral wall oscillations on turbulent boundary layer characteristics, particularly drag reduction. The experiments were performed in the same channel facilities as the present study, with the momentum thickness Reynolds number $Re_\theta \approx 1400$. Results were presented in Trujillo et al. (1997) for oscillation frequencies of $0.003 \le f^+ \le 0.018$, with the peak-to-peak amplitude varying over the range of $120 \le \Delta z^+ \le 360$. A maximum drag

reduction of 30% was found, and this drag reduction was accompanied by decreases in $u'$, $v'$, and $-\overline{uv}$, compared to the stationary wall flow. Suppression of the bursts and sweeps near the wall was also found for the oscillating wall case, with much greater suppression of the stronger bursts and sweeps. In contrast to previous studies, the drag reduction was found to be a function of non-dimensional wall speed $W^+_{wp} = (\Delta z^+/2)\, 2\pi f^+$, rather than the oscillation frequency or amplitude.

Choi, DeBisschop and Clayton (1998) performed a wind tunnel experiment to investigate the changes in the turbulent boundary-layer structure with a lateral wall oscillation. The Reynolds number based on the momentum thickness was $Re_\theta \approx 1190$. The oscillation frequencies examined ranged from $0.002 \leq f^+ \leq 0.014$, with the peak-to-peak amplitude being $\Delta z^+ \approx 490$. Their results clearly showed that turbulence intensities were reduced by the spanwise-wall oscillation. At the maximum wall oscillation velocity, skin-friction reduction of as much as 45% was observed within five boundary-layer thicknesses downstream of the leading edge. However, surprisingly some drag reduction was also discovered at two boundary-layer thicknesses upstream from the leading edge of the oscillating surface.

All the previous studies considered only a single Reynolds number. Furthermore, computational studies have been at very low Reynolds numbers, below $Re_\theta = 360$, whereas experimental studies have had $Re_\theta \geq 1000$. Consequently a major objective of the present study was to determine the Reynolds number effect on the drag reduction. Experiments were carried out from $Re_\theta = 500$ to $Re_\theta = 2400$. None of the previous studies have established the saturation point of the drag reduction as a function of both oscillating frequency and amplitude. This was another objective of the present study. The drag reduction along the streamwise distance was also of interest in the present study. The minimum distance for the drag reduction to be fully effective and the distance for the drag reduction effect to die out were both examined and established. Finally, numerical simulations were developed and used to determine details of the physical mechanisms causing drag reduction.

## Experimental Program

Experiments were conducted in a water channel facility that was modified to incorporate an oscillating wall. Velocity field measurements of all three velocity components were made with LDV systems, and near-wall single component measurements were made with hot-film anemometry. These measurements yielded drag reduction, mean velocity profiles, and normal and shear Reynolds stresses. Furthermore, conditional sampling was used to study the effects on burst and sweep structures. Flow visualization was also incorporated to determine the effects on turbulence structures.

### *Water channel facility and instrumentation*

All the experiments for this study were conducted in a low-speed, free-surface, recirculating water channel Figure 1. This facility has been operational in our laboratory for a number of years, and was modified for this study to incorporate an oscillating wall section. The channel facility included upstream and downstream stilling tanks, a test section, oscillating wall section, two pumps to control the recirculation, and two 200-gallon storage tanks. The channel was constructed of 1.27cm thickness cast acrylic sheeting. One of the side walls at a downstream station of the test section was constructed of glass to improve optical access for LDV measurements.

The flow entered the test section through a smooth inlet contraction. The test section was 5m long, 50cm wide and 30cm high. A false floor with the same height as the oscillating wall was installed through the entire length and width of the test section to provide clearance for mechanical elements associated with the oscillating-wall system. A 3mm diameter rod was mounted on the test floor 50cm downstream from the entrance to trip the boundary layer to a turbulent boundary layer flow.

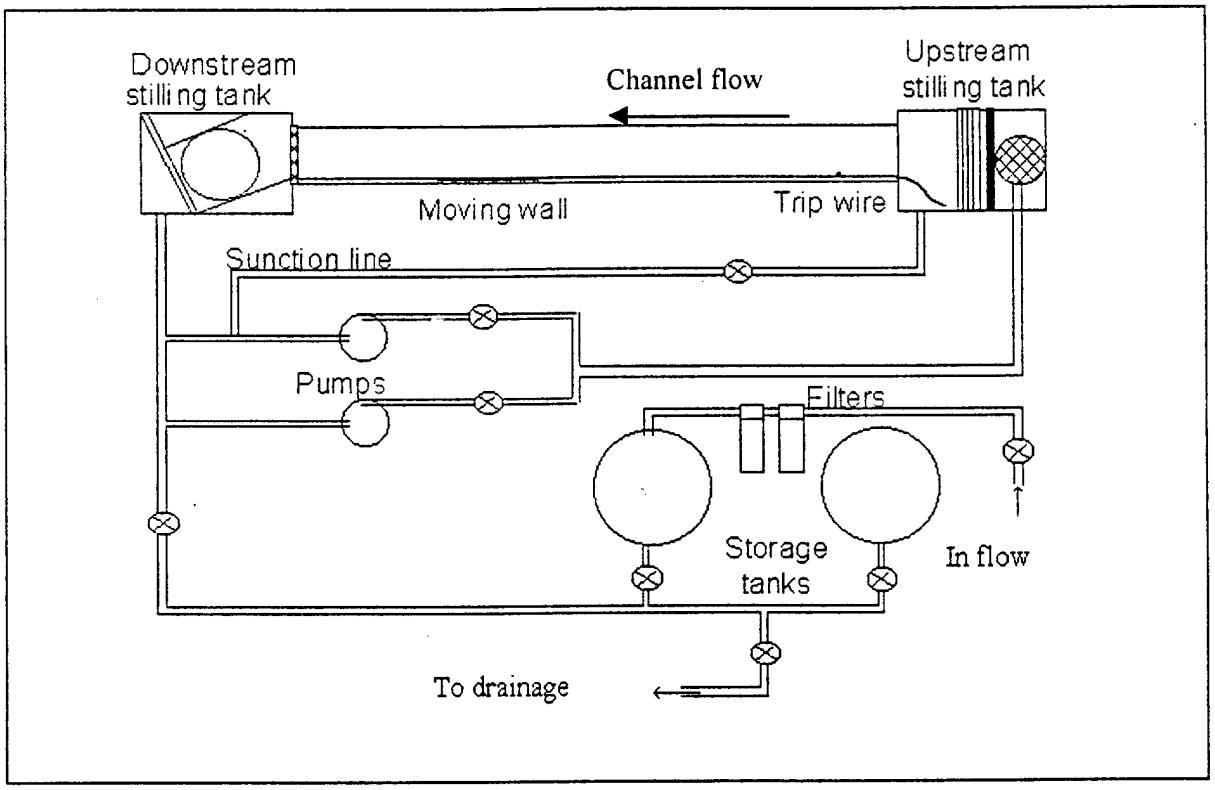


Figure 1. Schematic of water channel facility.

A 660mm long × 450mm wide oscillating wall section was installed 3.5 m downstream of the test section inlet. Details of the oscillating wall system are presented in the dissertation of Trujillo (1999). The motion of the wall was driven by a computer controlled stepping motor. The stepping motor was connected to the moving wall by a crank-slider mechanism, resulting in a nearly sinusoidal motion, with the maximum deviation from a true sinusoidal curve of approximately ±3%. The amplitude of the oscillation ranged from 12 mm to 48 mm, and the frequency was varied from 0.12 Hz to 2.5 Hz with a free-stream velocity of $U_\infty$ = 0.18 m/s, water depth of 200 mm, boundary layer thickness at the measurement position of $\delta$ = 60 mm, momentum thickness of $\theta$ = 7.5 mm, and friction velocity of $u_\tau$ = 8.5 mm/s.

Two different LDV systems were used in this present study. One was a TSI four-beam two-component LDV system used in back-scatter mode to measure streamwise and wali normal velocity components. The second was an in-house built fiber-optic based system, using side-scatter collection, designed to measure streamwise and lateral velocity components close to the wall ($y^+ \approx 3$ to 4, or within 0.3 mm of the wall). Signal processing was done using a TSI IFA-650 Burst Correlator. Hot-film measurements were done using a TSI model 1261-10W boundary layer probe operated with an A. A. Lab System AN-103 anemometer.

### *Measurement of drag reduction*

Two different techniques were used to estimate the drag reduction. First, the turbulence shear stress profile was measured near the wall ($y^+ < 30$) and the local wall shear stress calculated by summing the turbulence and viscous stresses near the wall. The second technique was to measure the mean velocity profile in the viscous sublayer, and the drag reduction found from the reduction of the mean velocity at a set height. For example, given that the velocity profile in the viscous sublayer (generally $y^+ < 5$) is linear, such that:

$$U^+ = y^+ \tag{1}$$

Also, since

$$\tau_w = \mu \, dU/dy = \mu \, U/y \tag{2}$$

The percentage reduction in drag is equal to the percentage decrease in mean velocity $U$. That is,

$$\Delta\tau_w / \tau_w = \Delta U / U \tag{3}$$

According to Durst *et al.* (1996), the velocity profile in the viscous sublayer does not exactly follow a linear trend. Using the linear equation requires a three to four percent correction for a position of $y^+ = 5$. However, the correction would apply for both the oscillation-wall case and the stationary-wall case, so the net effect on estimation of the drag reduction would be negligible.

## *Experimental results*

The effects of the oscillating wall on drag reduction, mean turbulence statistics, and turbulence structure, were studied for a range of oscillation amplitudes and frequencies. The effects of the wall oscillation on the velocity field characteristics were measured including profiles for $\overline{U}$, $u_{rms}$, $v_{rms}$, $w_{rms}$, and $\overline{uv}$. Measurements of these profiles were made at varying positions along the oscillating plate to establish what distance from the start of the oscillating plate was required to establish fully developed conditions. Phase averaged analyses of these measurements were also done based on the phase of oscillation of the plate. The effects on burst and sweep structure were studied using quadrant detection based on the $uv$ measurements. Results from these velocity field and turbulence structure measurements are presented in the dissertation by Trujillo (1999).

Drag reduction experiments were done with a range of free-stream velocities in order to obtain a range of Reynolds numbers. A summary of test conditions, and the resulting drag reduction is presented in Table 1. Results for drag reduction and effects on the velocity field and turbulence structure are presented for varying wall oscillation conditions, and Reynolds numbers, and positions on the oscillating surface in the following sections.

### *Drag reduction for varying wall oscillation amplitude and frequency*

The standard position for the drag reduction measurements listed in Table 1 was 420 mm downstream of the start of the oscillating plate, which corresponded to non-dimensional distances of $x/\delta_0 = 6.4$ or $x^+ = 4100$. By independently varying the amplitude and frequency of the wall oscillation, we were able to determine the functional dependence of drag reduction on these parameters. These results showed that the drag reduction is not dependent on the oscillation fequency, nor the oscillation amplitude, but rather the peak wall speed, i.e. $W^+_{wp} = (\Delta z^+/2)\cdot 2\pi\cdot f^+$. Drag reduction measurements at Reynolds number of $Re_\theta = 1400$ are shown in Figure 2 as a function of the peak wall speed. This figure shows a systematic trend of increasing drag reduction with increasing wall velocity. As shown in our paper, Trujillo et al. (1997), neither the oscillation frequency nor amplitude yield a consistent correlation with drag reduction.

Also shown on Figure 2 are the results from various previous experimental and computational simulation studies (it should be noted that Laadhari et al., 1994, did not present drag reduction values, but for comparison with our results we estimated the drag reduction for their experiments based on the mean velocity reduction near the wall presented in their paper). The general trend of increasing drag reduction found in previous studies was similar to that found in this study, but the level of drag reduction was generally less in this study. The drag reduction values presented in the experimental studies by Choi et al. (1998) were determined from hot-wire measurements close to the wall. Similarly, the drag reduction values for the

Table 1. Summary of drag reduction results

| $Re_\theta$ | $\Delta z$ (mm) | $\Delta z^+$ | $f$ (Hz) | $f^+$ | $W^+_{peak}$ | $DR$ |
|---|---|---|---|---|---|---|
| 500 | 48 | 200 | 0.12 | 0.009 | 5.4 | 20.0% |
| | | 200 | 0.25 | 0.019 | 11.2 | 27.9% |
| | | 200 | 0.37 | 0.028 | 16.6 | 27.1% |
| | | 200 | 0.5 | 0.038 | 22.5 | 28.5% |
| | | 200 | 0.75 | 0.057 | 33.7 | 28.1% |
| | | 200 | 1 | 0.075 | 45.0 | 27.3% |
| | | 200 | 1.25 | 0.094 | 56.2 | 27.9% |
| 950 | 36 | 240 | 0.2 | 0.005 | 4.0 | 11.0% |
| | | 240 | 0.4 | 0.011 | 8.1 | 21.7% |
| | | 240 | 0.7 | 0.019 | 14.1 | 29.7% |
| | | 240 | 0.8 | 0.021 | 16.1 | 27.7% |
| | | 240 | 0.9 | 0.024 | 18.2 | 29.1% |
| | | 240 | 1 | 0.027 | 20.2 | 29.3% |
| | | 240 | 1.2 | 0.029 | 22.2 | 27.3% |
| 1400 | 24 | 240 | 1 | 0.012 | 9.0 | 26.8% |
| | | 240 | 2 | 0.024 | 18.1 | 31.5% |
| | 36 | 360 | 0.25 | 0.003 | 3.7 | 5.4% |
| | | 360 | 0.5 | 0.006 | 7.1 | 14.9% |
| | | 360 | 0.75 | 0.009 | 10.7 | 22.5% |
| | | 360 | 1 | 0.013 | 14.3 | 28.9% |
| | | 360 | 1.25 | 0.016 | 17.9 | 31.3% |
| | | 360 | 1.5 | 0.020 | 22.2 | 30.5% |
| | | 360 | 1.75 | 0.023 | 25.9 | 30.1% |
| | 48 | 480 | 1.5 | 0.019 | 28.6 | 30.2% |
| | | 480 | 2 | 0.025 | 38.1 | 29.9% |
| | | 480 | 2.5 | 0.032 | 47.7 | 30.6% |
| | | 480 | 3 | 0.038 | 57.2 | 31.0% |
| 2400 | 36 | 800 | 0.6 | 0.003 | 6.7 | 16.0% |
| | | 800 | 1 | 0.004 | 11.2 | 25.5% |
| | | 800 | 1.6 | 0.007 | 17.9 | 29.2% |

Laadhari et al. (1994) were deduced based on the mean velocity measurement made with hot-wire measurements. We have shown (see Wu, 2000) that hot-wire measurements near oscillating walls are susceptible to errors due to the strong lateral velocities induced by the wall

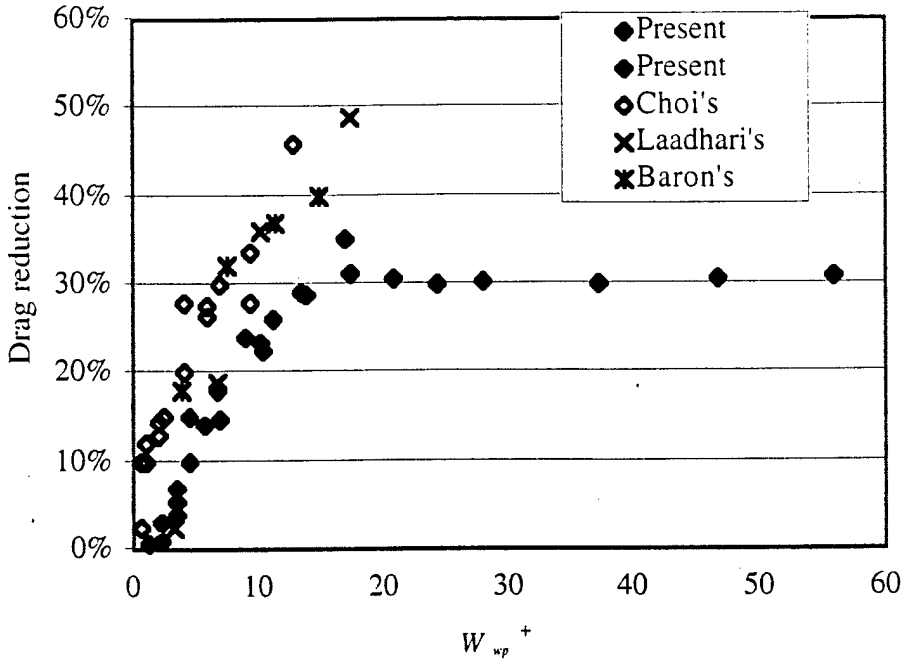


Figure 2. Drag reduction results from the current experimental measurements, and previous experimental and computational studies.

motion. Consequently the drag reduction determined from the LDV measurements used in this study are more reliable than previous hot-wire measurements.

An important result from this study is the clear evidence that the drag reduction reaches an asymptotic level with increasing wall oscillation velocity, with the maximum level occurring by approximately $W^+_{wp} = 12$. This result has not been recognized in previous studies because the maximum wall oscillation has not exceeded $W^+_{wp} = 17$ in any previous studies, whereas we have performed experiments with maximum wall oscillations up to $W^+_{wp} = 57$.

Note, although the current results are consistent with most previous experimental and computational studies of the effect of an oscillating wall on drag reduction, they are in direct contradiction to the numerical simulation results of Jung et al. (1992). Jung et al. investigated a range of oscillation frequencies for which the oscillation amplitude was varied so that the peak oscillation velocity remained constant. They found that at $W^+_{wp} = 12$, the drag reduction varied significantly with oscillation frequency, achieving a maximum 40% drag reduction for a nondimensional frequency of $f^+ = 0.01$. For the same range of nondimensional frequency we found that the drag reduction at $W^+_{wp} = 12$ was constant with a value slightly less than 30%.

*Drag reduction for varying Reynolds number*

In this study, four different Reynolds numbers were examined, ranging from $Re_\theta \approx 500$ to 2400. Reynolds numbers were adjusted by varying the free-stream velocity. Table 1 lists drag reduction results for varying Reynolds numbers, and these results are shown graphically in Figure 3. This figure clearly shows that there was no significant effect of Reynolds number on the drag reduction. All the drag reduction distributions followed the same trend and reached the same maximum drag reduction of approximately 30%. It is important to note that these results provide a critical link between the previous computational studies, which have been at very low Reynolds numbers ($Re_\theta < 360$), and experimental studies that previously had been at $Re_\theta > 1000$.

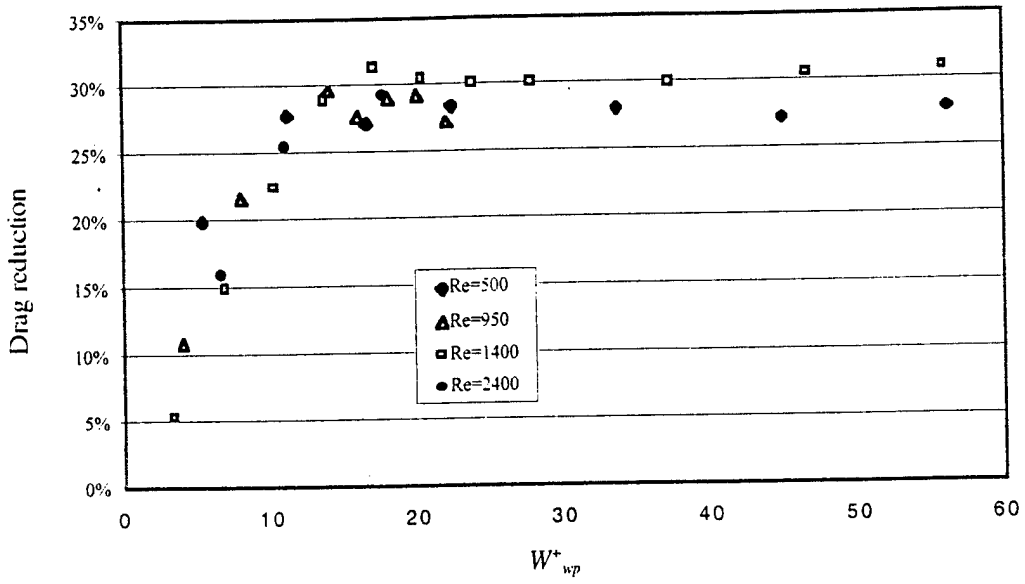


Figure 3. Reynolds number effect on drag reduction.

*Drag reduction at the leading edge and trailing edge of the oscillating wall*

The drag reduction as a function of position on the oscillating wall is shown in Figure 4. For these measurements the oscillation frequency was $f^+ \approx 0.015$ and the peak-to-peak amplitude was $\Delta z^+ \approx 240$, so the peak wall velocity was $W^+_{wp} \approx 9$. Hot-film measurements in the viscous sublayer were taken to estimate the drag reduction using corrections necessary for these hot-film measurements.

From Figure 4, it is evident that the drag reduction induced by the oscillation wall motion becomes fully effective within the distance of $3\delta_0$ ($x^+ \approx 2000$). Not surprisingly, there was no drag reduction immediately upstream of the oscillating plate, as evident by the measurement at $x \approx -0.4\delta_0$. At $x \approx 1\delta_0 (x^+ \approx 700)$, 18% drag reduction was already induced, indicating that a quick response to the imposed oscillation motion lies in the region close to the leading edge. The

disturbed flow structure adjusted to the new equilibrium state after $x \approx 3\delta_0$ and the drag reduction remains at the same level along the downstream of the plate. No significant difference was found in the mean velocity profiles as well as the turbulence properties behavior between the position of $x/\delta_0 \approx 4.2$ and $x/\delta_0 \approx 7$.

The drag reduction variation at the end and immediately downstream of the oscillating plate was also examined in the present study and the drag reduction profile with the distance from the trailing edge is also plotted in Figure 4. The drag reduction decreased rapidly following the trailing edge. At a location of $x \approx 1\delta_0$ from the trailing edge, only 5% drag reduction was observed.

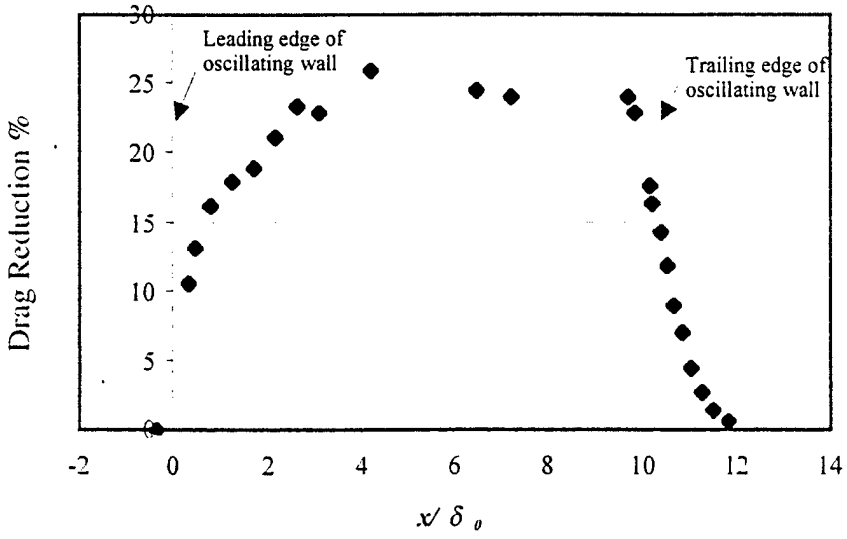


Figure 4. Variation of drag reduction along the oscillating test plate

## Computational Program

The computational component of this research involved modifying a DNS code to incorporate an oscillating surface in a duct flow. DNS computations were completed for a range of wall oscillation conditions, and the effects on the turbulence statistics and turbulence structure evaluated. The computational methodology and results from the DNS computations and analysis are described below.

### *Computational methodology*

Turbulent flows contain a wide range of length scales, bounded above by the geometric dimension of the flow field and bounded below by the dissipative action of the molecular viscosity. The nature of the current work requires that the numerical method being used is capable of resolving all relevant length scales in the flow. Therefore a Direct Numerical

Simulation (DNS) technique was used to perform this work. The ratio of the largest length scale $L$ to the smallest length scale $l$, usually known as the Kolmogorov scale, is

$$\frac{L}{l} = Re^{3/4} \tag{5}$$

As one can see from Equation 5, the range of length scales to be resolved increases as the Reynolds number increases, and so does the number of grid points needed in the computational model. Moreover, the total number of numerical operations required to compute a turbulent flow during a characteristic period of time is proportional to $Re^{11/4}$ (Canuto et al., 1988). Since the computational demand of DNS is so tremendously high, application of DNS methods is usually limited to low Reynolds number flow and relatively simple flow geometries.

In the course of this work simulations were performed for the turbulent flow in a rectangular duct. A duct was considered instead of a channel to circumvent questions that might arise due to the assumption of spanwise periodicity in the case of channel flow. Simulations focused on a duct with an aspect ratio of 6 (spanwise to wall-normal) and a length of $2\pi h$, where h is the duct height. Preliminary simulations had shown that for an aspect ratio of 6 the effect of the side walls on the flow in the center of the duct is negligible. Also, the duct was found to be long enough to establish a downstream flowfield that is uncorrelated with the inlet flow field. Periodic boundary conditions were imposed in the streamwise (x) direction. The Reynolds number for all simulations was $Re_\tau = 150$, based on the mean shear velocity and the duct half height. The size of the computational grid was 64x192x150 (wall-normal x spanwise x streamwise) grid points, and the non-dimensional time step size was $\Delta t = 0.0003$.

For the DNS a Fourier-Chebyshev collocation spectral method was used. A spectral method was chosen because of its storage and speed advantage compared to other methods, e.g. finite-difference methods. Although a finite-difference method is faster than a spectral method which uses the same number of grid points, the finite-difference method requires many more grid points to produce a comparably accurate solution, resulting in a lower overall speed (Canuto et al., 1988).

The incompressible three dimensional and time-dependent conservation equations were solved in a Cartesian coordinate system subject to imposed boundary conditions. To solve the conservation equations at each time step, a Fourier-Chebyshev collocation spectral method was used with no dealiasing. Relative to a pseudospectral method, the collocation method provides a simpler approach to specifying the boundary conditions, a slight improvement in convergence characteristics, and the elimination of the need to transfer back and forth between physical and wavenumber space (Canuto et al., 1988). The physical variables to be determined (velocities and pressure) were represented by truncated series expansions of Chebyshev polynomials on a Gauss-Lobatto grid in both spanwise (z) and wall-normal (y) non-periodic directions and by Fourier series on an evenly spaced grid in the periodic streamwise (x) direction.

To address the issue of the pressure-velocity coupling present in incompressible flows, an influence matrix technique was used. This approach is generally credited to Kleiser and Schumann (1980), who used it in a pseudospectral simulation of channel flow with one non-periodic direction. In a continuous representation of the Navier-Stokes equations, the influence matrix technique determines the pressures that ensure a divergence free condition throughout the solution domain by forcing the divergence of the velocities on the boundaries to be zero. For the discretized problem, additional corrections throughout the domain are needed to force the divergence to machine precision zero due to the fact that the momentum equations are not satisfied on the boundary. The technique including the correction for the boundary momentum residuals is described in detail by Tuckerman (1989) and Madabushi et al. (1993).

For the time discretization an Adams Bashford/second order backward Euler (AB/2BE) scheme was applied, giving an implicit treatment of the diffusion terms and an explicit treatment of the advection terms that is second order accurate in time (Ehrenstein and Peyret, 1989). At each time step, the solution proceeds by first calculating all source terms and transforming them to wavenumber space using a forward Fast Fourier Transform (FFT) in the periodic direction. Since the pressure boundary conditions are unknown, the pressure Poisson equation is first solved with homogenous boundary conditions to find a pressure field and then the momentum equations are solved. Then, using the predetermined influence matrix, the correct boundary pressures that will ensure a divergence-free velocity field are determined. Using these boundary pressures, the pressure Poisson equation is solved again followed by the solutions of the momentum equations to determine the final velocity components in wavenumber space at the new time step. This step-by-step procedure is taken, in turn, for each of the real and imaginary parts of the equations to be solved for each Fourier wavenumber. The physical quantities are then obtained by performing a backward FFT in the streamwise direction, in preparation for the calculation of the source terms for the next time step solution. The numerical algorithm is described in Hill and Ball (1999).

### *Computational Results*

Starting from the statistically steady solution for the stationary wall case, simulations were performed with active top and bottom walls. The center part $(-2 \le z/h < 2)$ of the walls were oscillated using a variety of frequencies and amplitudes. The Reynolds number was kept constant at $\mathrm{Re}_\tau = 150$, based on the mean shear velocity $u_{\tau 0}$ and the duct half height.

Effective drag reduction was determined in the center part of the duct flow for various wall oscillation frequencies and amplitudes. Results were similar to the experimental results discussed previously, except a maximum drag reduction of 40% was obtained for the maximum peak wall oscillation velocity of $W^+_{wp}$ = 30 computed for the DNS. The computational predictions also showed a suppression of $u_{rms}$, $v_{rms}$, $w_{rms.}$ and $\overline{uv}$ values similar to the experimental measurements.

Of particular interest in this study was the effect of wall oscillations on turbulence structure. Flow visualization in the experimental program showed that the characteristic near-wall streak structure was strongly suppressed by the wall oscillation. Experiments using flow visualization and velocity field measurements also showed a suppression of bursts and sweeps farther from the wall. Consequently, the DNS flow field was analyzed to determine if similar effects on turbulence structure were predicted. Furthermore, the DNS allowed more comprehensive analysis of these effects.

An indication of the streak structure is given in Figure 5 showing the distribution of the fluctuating velocity component $u'$, non-dimensionalized by $u_{\tau 0}$ (the friction velocity for the stationary case), in an $x$-$z$-plane is shown at a height of $y^+ = 6.5$ from the bottom wall.

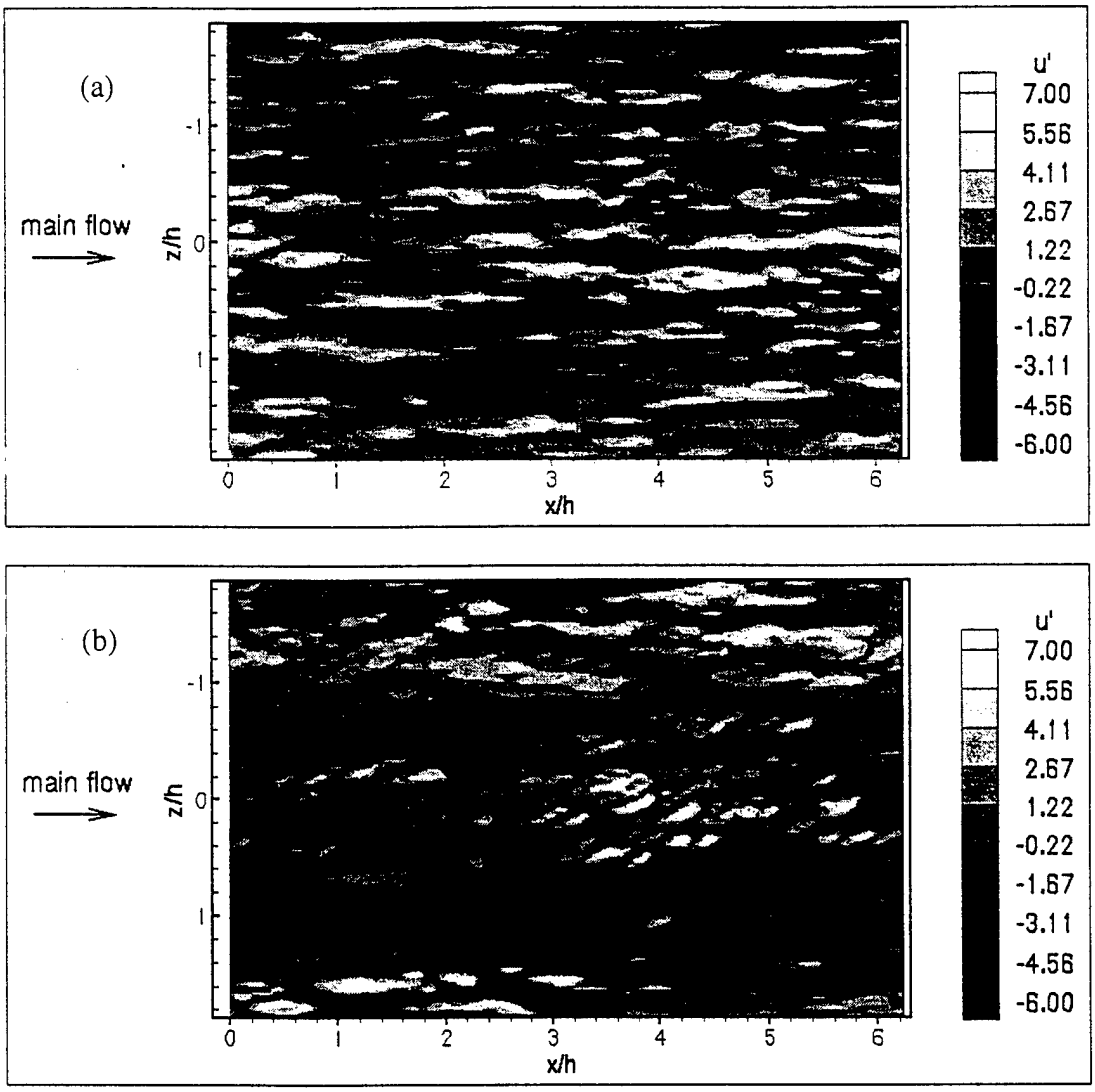


Figure 5: Contours of fluctuating velocity component $u'$ close to bottom wall ( $y^+ = 6.5$); (a) stationary wall; (b) oscillating wall (peak wall speed $W^+_{wp} = 7.5$ ).

Note that only the center part (in spanwise direction) of the duct is shown. In the stationary wall case, which is represented Figure 5 (a), the well known pattern of alternating high and low speed streaks can be seen. The active wall case is shown in Figure 5 (b). The oscillation frequency for this case was $f\nu/u_\tau^2 = 0.01$ and the amplitude was $bu_\tau/\nu = 120$, giving a peak wall speed of $W_p^+ = 7.5$. In this case the near-wall layer appears to be much more homogenous in the region next to the oscillating wall. The motion of the wall clearly affects the flow structure in the near-wall layer, homogenizing it and suppressing the development of streaks.

To obtain a more direct comparison with our experimental flow visualization, the paths of tracer particles introduced along a line across the flow were calculated. This calculation simulated hydrogen bubble flow visualization. Figure 6 shows representative patterns of tracer particles. The massless tracer particles were inserted into the flow field at 129 insertion points that were evenly distributed in the center region of the duct, $-1.5 \le z/h \le 1.5$, at $x/h = 0$ and at a distance from the wall of $y^+ = 6.5$. The paths of the particles were then calculated based on the flow velocities at their current locations and the time step $\Delta t$. Fig. 2 shows instantaneous snapshots of the particle distribution in the flow field at a time of $tu_\tau^2/\nu = 45$ after inserting the first row of particles. The flow direction is from the top to the bottom. Figure 6 (a) represents the stationary wall case, and shows that the particles, after being inserted evenly, are transported laterally and form well defined streaks as they move downstream. The lateral motion of the particles is due to streamwise vortices. The center of the streamwise vortical structures is located on average at a height of $y^+ \approx 20$ with a radius of $r^+ \approx 15$ (Kim et al., 1987). Hence the bottom of these vortices with the spanwise velocity component being the dominant component is located in the near-wall sublayer, causing the lateral transport of the tracer particles.

Figure 6 (b) shows the oscillating wall case. For the case shown here the oscillation frequency was $f\nu/u_\tau^2 = 0.01$ and the amplitude was $bu_\tau/\nu = 240$, resulting in a peak wall speed of $W_p^+ = 15.1$. Insertion of particles was started at the beginning of the oscillation period, i.e. the phase of the oscillation was $\varphi = 0$ and the wall speed was $W^+ = 0$. In Figure 6 (b) the particle distribution at a time of $t^+ = 45$ after the beginning of the oscillation period is shown. Since the duration of one oscillation period is $100\,t^+$ the snapshot in Figure 6 (b) shows the flow field in the first half of the period when the wall is moving in positive $z$-direction. Due to the viscous shear the fluid in the vicinity of the wall is moving in positive $z$-direction as well, which causes the tracer particles to be shifted to the right. However, there is a phase lag for the flow at $y^+ = 6.5$ so that the flow is still moving to the right at the instant shown in Figure 6 although the wall is stationary at this time. The distribution of particles is much more homogeneous for the oscillating wall than in the stationary wall case. Apparently the wall oscillation suppresses the development of streamwise vortical structures.

Figure 7 shows endviews of the tracer particle field. In this case particles were inserted at three different heights, namely $y^+ = 6.5$, $y^+ = 18$ and $y^+ = 30$. Only particles at a distance of

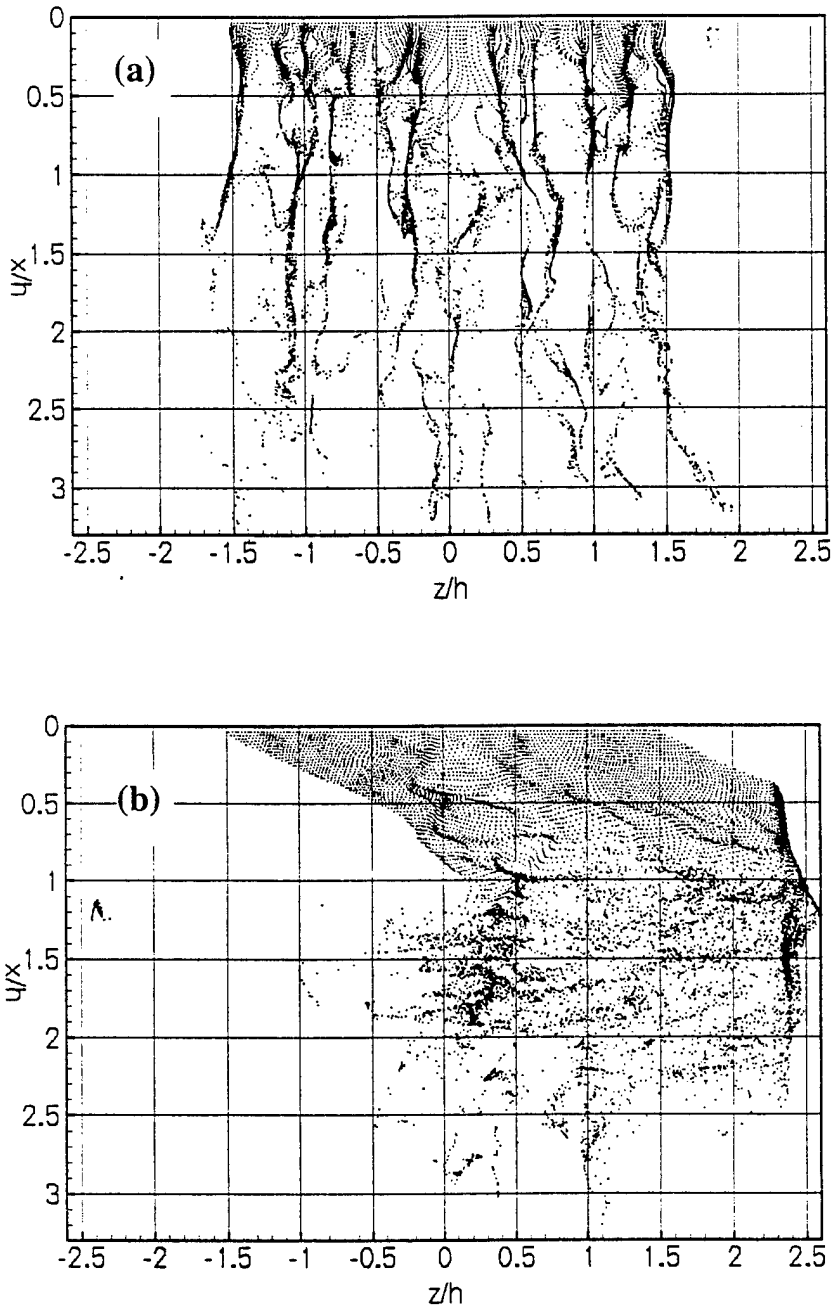


Figure 6: Patterns of tracer particles inserted at $y^+ = 6.5$ ; (a): stationary case; bottom: oscillating case.

$\Delta x^+ = 150 - 180$ downstream of the insertion point are shown in Figure 7. Note also that the scale of the two axes is y:z = 5:1. In the stationary wall case, shown in Figure 7 (a), it can be observed that the originally straight rows of particles are vigorously distorted due to upward and downward moving fluid. These effects are commonly known as ejections and sweeps,

respectively. In the oscillating wall case, shown in Figure 7(b), the rows of particles appear to be much smoother. In fact, the particles inserted next to the wall at a height of $y^+ = 6.5$ still form a straight line. In this area the oscillating wall appears to prevent the formation of ejection and sweeps, while their formation in the upper part of the boundary layer is suppressed.

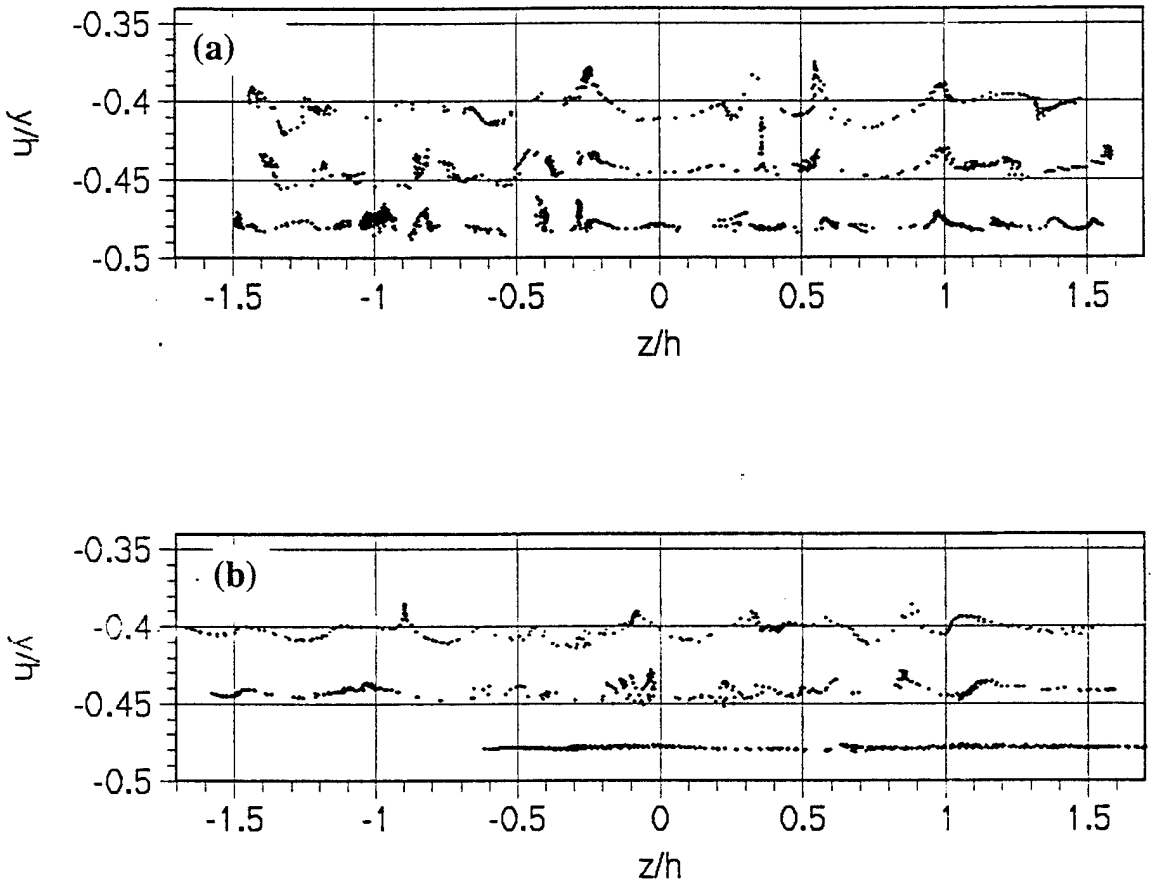


Figure 7: Endviews of tracer particles at $\Delta x^+ = 150 - 180$ downstream of insertion point; (a): stationary wall; (b): oscillating wall.

## Conclusions

This research program used experimental and computational simulations to study the drag reduction, and the resulting effects on turbulence structure, for a turbulent wall flow subjected to lateral wall oscillations. Major objectives for this study were to establish wall oscillation conditions resulting in maximum drag reduction, and how the turbulence structure was altered so that this drag reduction was attained. Furthermore we were interested in the drag reduction performance over a range of Reynolds numbers, and the onset of the drag reduction at the start of the oscillating wall section, and the decay of drag reduction downstream of the oscillating wall.

Our experiments showed the maximum drag reduction for an oscillating wall is 30%. Furthermore, the drag reduction reaches an asymptotic level with increasing wall oscillation velocity, with the maximum level occurring by approximately $W^+_{wp} = 15$. This result has not been recognized in previous studies because the maximum wall oscillation has not exceeded $W^+_{wp} = 17$ in any previous studies, whereas we have performed experiments with maximum wall oscillations up to $W^+_{wp} = 57$. Drag reduction performance was tested for Reynolds numbers of $Re_\theta = 500$, 950, 1400 and 2400, and the performance was found to be independent of Reynolds number for this range. This result is particularly important since the lowest Reynolds number tested was close to that used in DNS computations which are inherently limited to low Reynolds numbers. Consequently this result shows that the DNS studies completed as part of this research program, and previous DNS studies are applicable to significantly larger Reynolds numbers.

Experimental and computational studies of the turbulence structure showed the oscillating wall has dramatic effect in practically eliminating the streak structures. Furthermore, the burst and sweep structures were suppressed. The results presented in this report highlighted the effects on the streak structure. More detailed analysis of the effects on burst and sweep structures presented in the dissertation by Trujillo (1999) and the thesis by Ricco (2000) describe a dramatic reduction of "strong" bursts and sweeps which extends much farther from the wall than the immediate effects of the wall oscillation. We conclude from this result that the wall oscillation suppresses the rejuvenation mechanisms for burst and sweeps by displacing the accumulation of low speed fluid in the wall region from the over-riding quasi-streamwise vortices.

## *References*

Baron A. and Quadrio M. 1996 Turbulent drag reduction by spanwise wall oscillations. *Applied Scientific Research* 55 311.

Canuto, C., Hussaini, M.Y., Quarteroni, A. and Zang, T.A., 1988. *Spectral Methods in Fluid Dynamics*. Springer-Verlag.

Choi K-S., DeBisschop J-R. and Clayton B.R. 1998 Turbulent Boundary-layer control by means of spanwise-wall oscillation *AIAA Journal* Vol. 36. No. 7, 1157.

Durst, F., Kikura, H., Lekakis, I., Jovanovic, J., and Ye, Q., 1996 Wall shear stress determination from near-wall mean velocity data in turbulent pipe and channel flows. Physics of Fluids, Vol. 20, 417

Ehrenstein, U. and Peyret, R.A., 1989. A Chebyshev-collocation method for the Navier-Stokes equations with application to double-diffusive convection. *Int. J. Numer. Methods Fluids,* 9, 427.

Hill, R.W. and Ball, K.S., 1999. Parallel implementation of a Fourier- Chebyshev collocation method for incompressible fluid flow and heat transfer. *Numerical Heat Transfer, Part B,* 36 (3), 309-329.

Jung, W.J., Mangiavacchi N. and Akhavan R. 1992 Suppression of turbulence in wall-bounded flows by high-frequency spanwise oscillations. *Physics of Fluids* A 4 (8) 1605.

Kim, J., Moin, P. and Moser, R., 1987. Turbulence statistics in fully developed channel flow at low Reynolds number. *J. Fluid Mech.,* 177, 133-166.

Kleiser, L., Schumann, U., 1980. Treatment of incompressibility and boundary conditions in 3-D numerical spectral simulations of plane channel flows. Proc. *3rd GAMM Conf. Numer. Methods Fluid Mech.*, Vieweg Braunschweig, 165.

Laadhari, F., Skandaji, L. and Morel, R., 1994. Turbulence reduction in a boundary layer by a local spanwise oscillating surface. Physics of Fluids, Vol. 6, 3218-3220.

Madabushi, R.K., Balachandar, S. and Vanka, S.P., 1993. A divergence-free Chebyshev collocation procedure for incompressible flows with two non-periodic directions. *Journal of Computational Physics*, 105, 199.

Ricco, P. A., 2000. Flow visualization and velocity measurements of a turbulent boundary layer modified by spanwise oscillations. . M.S. thesis, The Univ. of Texas at Austin.

Trujillo, S.M. Bogard, D.G. and Ball, K.S., 1997. Turbulent boundary layer drag reduction using an oscillating wall. *28th AIAA Fluid Dynamics Conference, 4th AIAA Shear Flow Control Conference,* Snowmass Village, CO.

Trujillo, S.M., 1999. An investigation of the effects of spanwise wall oscillation on the structure of a turbulent boundary layer. Ph.D. dissertation, The Univ. of Texas at Austin.

Tuckerman, L.S., 1989. Divergence-free velocity fields in non-periodic geometries. *Journal of Computational Physics*, 80, 403.

Wu, S., 2000. An investigation of the Reynolds number effect on the drag reduction by spanwise wall oscillation. M.S. thesis, The Univ. of Texas at Austin.